Entanglement in a molecular three-qubit system

Amit Kumar Pal and Indrani Bose*
Department of Physics, Bose Institute,
93/1, A. P. C. Road, Kolkata - 700009

(Dated: November 9, 2018)

We study the entanglement properties of a molecular three-qubit system described by the Heisenberg spin Hamiltonian with anisotropic exchange interactions and including an external magnetic field. The system exhibits first order quantum phase transitions by tuning two parameters, x and y, of the Hamiltonian to specific values. The three-qubit chain is open ended so that there are two types of pairwise entanglement : nearest-neighbour (nn) and next-nearest-neighbour (nnn). We calculate the ground and thermal state concurrences, quantifying pairwise entanglement, as a function of the parameters x, y and the temperature T. The entanglement threshold and gap temperatures are also determined as a function of the anisotropy parameter x. The results obtained are of relevance in understanding the entanglement features of the recently engineered molecular Cr_7Ni-Cu^{2+}-Cr_7Ni complex which serves as a three-qubit system at sufficiently low temperatures.

PACS numbers: 03.67.Mn, 03.67.Bg, 03.65.Ud, 64.70.Tg, 75.10.Dg

I. INTRODUCTION

Entanglement is a unique feature of quantum mechanical systems with no classical analogue. In an entangled state, two or more quantum particles have joint properties in the form of non-local correlations rather than individual identities. Entanglement is known to be a key resource in quantum information processing (QIP) tasks such as quantum computation, teleportation and cryptography [1]. Implementation of QIP protocols requires the assembly of multi-qubit systems with the potential for generating controlled entanglement. Natural examples of qubits, which are two-level systems, include spin-$\frac{1}{2}$ particles, photons with two states of polarization and trapped ions with two atomic states. In recent years, molecular nanomagnets have been proposed as appropriate candidates for qubit encoding and manipulation [2, 3]. A specific example is provided by antiferromagnetic (AFM) Cr_7Ni rings which reduce to effective spin-$\frac{1}{2}$ systems at low temperatures. Each octagonal ring consists of one Ni^{2+} and seven Cr^{3+} ions with AFM coupling between neighbouring ions. A variety of experimental techniques have been used to characterize the rings. The rings have spin-$\frac{1}{2}$ ground states and behave as qubits at sufficiently low temperatures as the excited-state multiplets remain unoccupied. Also the rings have been demonstrated to possess long decoherence times, an ideal requirement for several QIP tasks.

Recently, Timco *et al* [3] have engineered a coherent coupling between two Cr_7Ni rings, serving as molecular spin qubits, via a central Cu^{2+} ion which acts as a third qubit. The Cr_7Ni-Cu^{2+}-Cr_7Ni complex is equivalent to a three qubit system with the Cu^{2+} ion serving as a "linker". The coupling between the spins of the rings is tunable by a proper choice of the linker. In a microscopic approach, the spin Hamiltonian describing the three-qubit system can be written as [3]

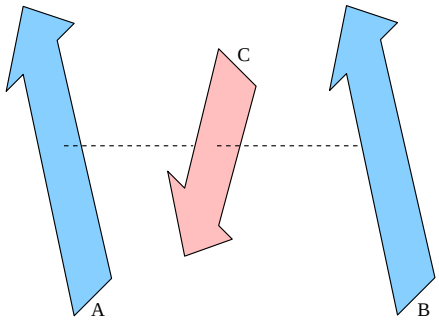

Figure 1: A molecular three-qubit system in which the qubits A and B represent two Cr_7Ni rings (see figure 1(a) of reference [3]) and qubit C represents the bridging ion Cu^{2+}. The rings and the ion are effective spin-$\frac{1}{2}$ systems represented by solid arrows.

$$H = H^A + H^B + H^C + H^{AC} + H^{BC} \tag{1}$$

where the labels A, B and C correspond to the two rings and the magnetic linker respectively. The terms H^A and H^B individually describe the Cr_7Ni rings:

$$H^A = H^B = \sum_{i=1}^{8} J_i \overrightarrow{S}_i . \overrightarrow{S}_{i+1} + \sum_{i=1}^{8} d_i S_{i,z}^2 + H_{dip} + \mu_B \overrightarrow{B} . \sum_{i=1}^{8} \overrightarrow{g_i} . \overrightarrow{S}_i \tag{2}$$

with z along the ring axis. The successive terms in the Hamiltonian correspond to isotropic exchange (J_i), axial crystal field (d_i), dipole-dipole couplings (H_{dip}) between eight individual spins $\overrightarrow{S}_i$ and the Zeeman coupling to the

*Electronic address: indrani@bosemain.boseinst.ac.in

magnetic field $\overrightarrow{B}$ with $\overrightarrow{\overrightarrow{g_i}}$ being the gyromagnetic tensor. The term H^C in equation (1) is

$$H^C = \overrightarrow{B}.\overrightarrow{\overrightarrow{g}}_{Cu}.\overrightarrow{S}_{Cu} \tag{3}$$

whereas the terms H^{AC}/H^{BC} are:

$$H^{AC} = H^{BC} = J'\overrightarrow{S}_{Cu}.\left(\overrightarrow{S}_{Cr} + \overrightarrow{S}_{Ni}\right) \tag{4}$$

where the spins $\overrightarrow{S}_{Cr}$ and $\overrightarrow{S}_{Ni}$ correspond to $\overrightarrow{S}_1$ and $\overrightarrow{S}_8$ in their respective rings as these spins are located on the edge of the octagon bound to the Cu link. Since $J' << J_i$'s, the intra-ring exchange constants, the low-temperature behaviour of the Cr_7Ni-Cu^{2+}-Cr_7Ni complex is determined by the splitting of the lowest eight energy levels. The behaviour can be reproduced in terms of an effective three-spin Hamiltonian [3]:

$$H = \bar{J}\sum_{i=A,B}\vec{S}_i.\vec{S}_C + \mu_B\overrightarrow{B}.\sum_{i=A,B,C}\overrightarrow{\overrightarrow{g_i}}.\overrightarrow{S}_i$$
$$+D_{ex}\sum_{i=A,B}(2S_{i,z}S_{C,z} - S_{i,x}S_{C,x} - S_{i,y}S_{C,y}) \tag{5}$$

where $\overrightarrow{S}_{A,B,C}$ represent spin-$\frac{1}{2}$ operators, $\bar{J}$ is the strength of the effective Cu-ring isotropic exchange, $\overrightarrow{\overrightarrow{g}}_{A,B}$ are the g-tensors of the ring ground doublet, $\overrightarrow{\overrightarrow{g}}_C = \overrightarrow{\overrightarrow{g}}_{Cu}$, and D_{ex} is an effective Cu-ring axial exchange originating from the projection of the rings' dipolar and crystal-field anisotropies. Equation (5) represents the Cr_7Ni-Cu^{2+}-Cr_7Ni system as a linear chain of three coupled qubits with open boundaries. The three-qubit system has ground and thermal states which are entangled. One can focus on two types of entanglement : pairwise, i.e. between two qubits and three-party entanglement involving all the three qubits. The Greenberger-Horne-Zeilinger (GHZ) and Werner (W) states [4, 5, 6] defined as

$$\begin{aligned}|GHZ\rangle &= \tfrac{1}{\sqrt{2}}\left(|\uparrow\uparrow\uparrow\rangle + |\downarrow\downarrow\downarrow\rangle\right)\\ |W\rangle &= \tfrac{1}{\sqrt{3}}\left(|\uparrow\uparrow\downarrow\rangle + |\uparrow\downarrow\uparrow\rangle + |\downarrow\uparrow\uparrow\rangle\right)\end{aligned} \tag{6}$$

represent two fundamentally non-equivalent entangled states of three qubits. In the first case, the pairwise entanglement for all the qubit pairs is zero and one has genuine three party entanglement known as the residual entanglement. The nomenclature arises from the Coffman-Kundu-Wootters (CKW) inequality [7] for a three qubit system given by,

$$\tau_1 \geq \tau_2 = \sum_{j\neq i} C_{ij}^2 \tag{7}$$

where τ_1 represents the one-tangle corresponding to the entanglement between the ith qubit and the rest of the system and C_{ij}^2 is the square of concurrence, a measure of the entanglement between the ith and jth qubits. The one-tangle τ_1 is determined as $\tau_1 = 4det\rho^{(1)}$ where $\rho^{(1)}$ is the single-site reduced density matrix. The residual entanglement is given by the difference between τ_1 and τ_2 and hence provides a measure of quantum correlations which cannot be expressed in terms of pairwise correlations. The GHZ state has the maximum possible value of 1 for the three-party (residual) entanglement. The W state, on the other hand, possesses only pairwise entanglement between all qubit pairs and the magnitude of the residual entanglement is zero. Timco *et al* [3] have provided a prescription for the generation of GHZ and W states using a sequence of microwave pulses applied to the molecular three-qubit system.

In this paper, we study the entanglement properties of the ground and thermal states of the molecular three-qubit system described by the reduced Hamiltonian in equation (5). We specially focus on the variation of entanglement measures as a function of the parameters of the Hamiltonian. Wang *et al* [8] have earlier studied thermal entanglement in the three-qubit Heisenberg XXZ model. The Hamiltonian considered by them satisfies periodic boundary condition and includes anisotropic exchange interaction and magnetic field terms. The molecular three qubit system considered in this paper has the structure of an open chain and the entanglement features turn out to be different from those of the three-qubit Heisenberg ring. The experimental demonstration that the coupling between the molecular spin clusters can be controlled without disturbing the intra-cluster interactions provides the impetus for characterizing the entanglement properties of the molecular three-qubit system.

II. GROUND STATE ENTANGLEMENT

We consider the molecular three-qubit system to be in an external magnetic field pointed in the z direction. The Hamiltonian (equation (5)) then reduces to

$$H = \bar{J}\sum_{i=A,B}\vec{S}_i.\vec{S}_C + g\mu_B B\sum_{i=A,B,C}S_i^z$$
$$+D_{ex}\sum_{i=A,B}(2S_{i,z}S_{C,z} - S_{i,x}S_{C,x} - S_{i,y}S_{C,y}) \tag{8}$$

This can be rewritten in the form,

$$\begin{aligned}\bar{H} = H/\bar{J} &= (1+2x)\left(S_{A,z}S_{C,z} + S_{B,z}S_{C,z}\right)\\ &+\frac{1}{2}(1-x)\left(S_A^+S_C^- + S_A^-S_C^+ + S_B^+S_C^- + S_B^-S_C^+\right)\\ &+y\left(S_{A,z} + S_{B,z} + S_{C,z}\right)\end{aligned} \tag{9}$$

where $x = D_{ex}/\bar{J}$, $y = g\mu_B B/\bar{J}$ and S^+, S^- are the raising and lowering operators. Since the z-component of the total spin, S_z^{tot}, is a conserved quantity, the eigenvalue problem can be solved in the separate subspaces corresponding to the different values of S_z^{tot}. The eigenvalues and the eigenstates are given by,

$\underline{S_z^{tot} = +\frac{3}{2}}$

$$|\psi_1\rangle = |\uparrow\uparrow\uparrow\rangle$$
$$E_1 = \tfrac{1}{2}(1 + 2x + 3y) \tag{10}$$

$\underline{S_z^{tot} = +\frac{1}{2}}$

$$|\psi_2\rangle = \tfrac{1}{\sqrt{2}}(-|\uparrow\uparrow\downarrow\rangle + |\downarrow\uparrow\uparrow\rangle)$$
$$E_2 = \tfrac{y}{2} \tag{11}$$

$$|\psi_3\rangle = \tfrac{1}{A(x)}(|\uparrow\uparrow\downarrow\rangle - R(x)|\uparrow\downarrow\uparrow\rangle + |\downarrow\uparrow\uparrow\rangle)$$
$$E_3 = \tfrac{1}{4}\{\, 2y - U_+(x)\} \tag{12}$$

$$|\psi_4\rangle = \tfrac{1}{B(x)}(|\uparrow\uparrow\downarrow\rangle - S(x)|\uparrow\downarrow\uparrow\rangle + |\downarrow\uparrow\uparrow\rangle)$$
$$E_4 = \tfrac{1}{4}\{\, 2y - U_-(x)\} \tag{13}$$

$\underline{S_z^{tot} = -\frac{1}{2}}$

$$|\psi_5\rangle = \tfrac{1}{A(x)}(|\downarrow\downarrow\uparrow\rangle - R(x)|\downarrow\uparrow\downarrow\rangle + |\uparrow\downarrow\downarrow\rangle)$$
$$E_5 = \tfrac{1}{4}\{\, -2y - U_+(x)\} \tag{14}$$

$$|\psi_6\rangle = \tfrac{1}{B(x)}(|\downarrow\downarrow\uparrow\rangle - S(x)|\downarrow\uparrow\downarrow\rangle + |\uparrow\downarrow\downarrow\rangle)$$
$$E_6 = \tfrac{1}{4}\{\, -2y - U_-(x)\} \tag{15}$$

$$|\psi_7\rangle = \tfrac{1}{\sqrt{2}}(-|\downarrow\downarrow\uparrow\rangle + |\uparrow\downarrow\downarrow\rangle)$$
$$E_7 = -\tfrac{y}{2} \tag{16}$$

$\underline{S_z^{tot} = -\frac{3}{2}}$

$$|\psi_8\rangle = |\downarrow\downarrow\downarrow\rangle$$
$$E_8 = \tfrac{1}{2}(1 + 2x - 3y) \tag{17}$$

In the above equations,

$$U_\pm(x) = \left\{\, 1 + 2x \pm \sqrt{3\,(4x^2 - 4x + 3)}\right\} \tag{18}$$

$$R(x) = \frac{-U_+(x)}{2(-1+x)} \tag{19}$$

$$S(x) = \frac{-U_-(x)}{2(-1+x)} \tag{20}$$

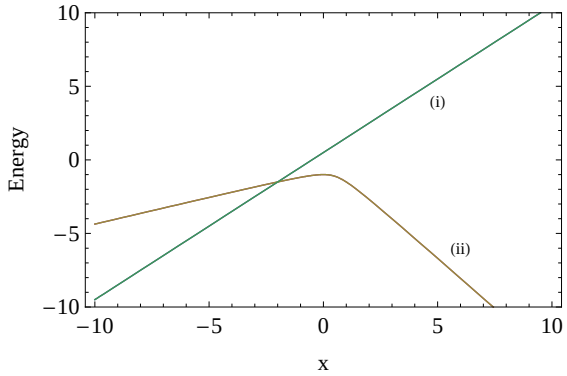

Figure 2: Two lowest energy levels (i) E_1 and E_8 and (ii) E_3 and E_5 of the Hamiltonian (equation (9)) versus the parameter x for $y = 0$.

$$A(x) = \left[2 + \left\{\frac{-U_+(x)}{2(-1+x)}\right\}^2\right]^{\frac{1}{2}} \tag{21}$$

$$B(x) = \left[2 + \left\{\frac{-U_-(x)}{2(-1+x)}\right\}^2\right]^{\frac{1}{2}} \tag{22}$$

We first consider the case of zero magnetic field (y=0). The eigenvalues then become

$$E_1 = E_8 = \tfrac{1+2x}{2}$$
$$E_2 = E_7 = 0$$
$$E_3 = E_5 = \tfrac{-U_+(x)}{4}$$
$$E_4 = E_6 = \tfrac{-U_-(x)}{4} \tag{23}$$

We assume x to range over both positive and negative values. Figure 2 shows a plot of the two lowest energy levels of the Hamiltonian (equation (9)) versus the parameter x. Each energy level is doubly-degenerate. The nature of the ground states change at $x = -2$, bringing about a first-order quantum phase transition (QPT). When x is < -2, the ground states are the separable states $|\psi_1\rangle$ and $|\psi_8\rangle$. When x is > -2, the doubly-degenerate ground state is described by the wave functions $|\psi_3\rangle$ and $|\psi_5\rangle$. At $x = 1$, however, the Hamiltonian (9) becomes Ising-like, i.e., loses its quantum character and the degenerate ground states, $|\uparrow\downarrow\uparrow\rangle$ and $|\downarrow\uparrow\downarrow\rangle$, are separable. We now discuss the entanglement properties of the ground states. Because of the degeneracy, the ground state density matrix describes a mixed state with

$$\rho = \frac{1}{2}\left(|\psi_3\rangle\langle\psi_3| + |\psi_5\rangle\langle\psi_5|\right) \tag{24}$$

The reduced density matrix ρ_{ij}, $(i, j = A, B, C)$ is obtained from ρ by tracing out the spin degrees of freedom associated with the spins which are not located at the sites i and j. The reduced density matrix in the stan-

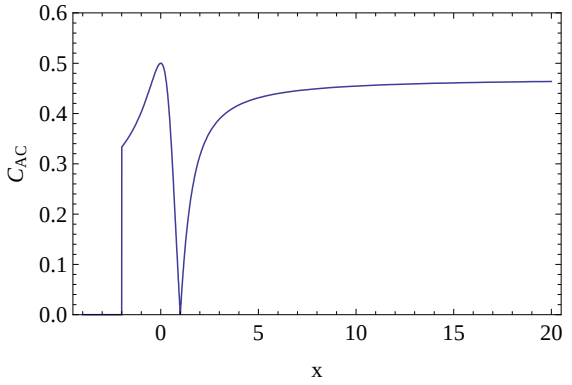

(a)

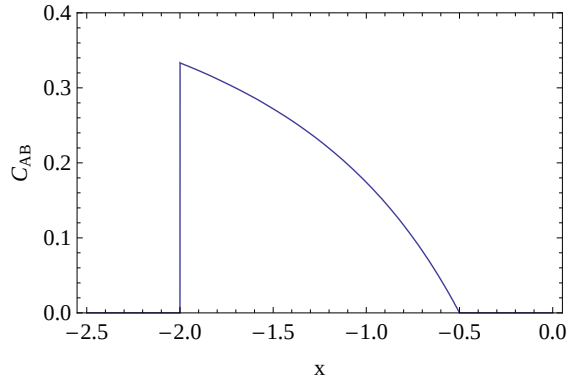

(b)

Figure 3: Variation of concurrences (a) C_{AC} and (b) C_{AB} versus x for $y = 0$.

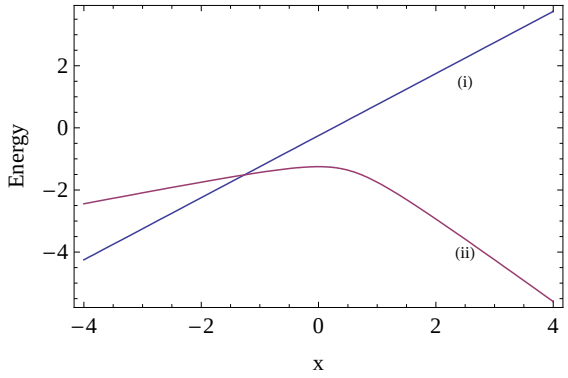

Figure 4: Plot of the two lowest energies (i)E_8 and (ii)E_5 versus x for $y = 0.5$.

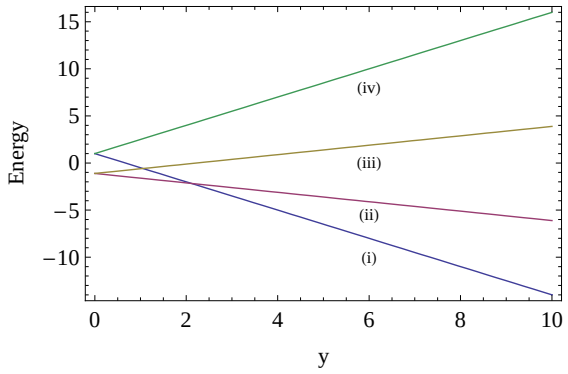

Figure 5: Plot of the lowest energy levels (i)E_8, (ii)E_5, (iii)E_3 and (iv)E_1 as a function of y for $x = 0.5$

dard basis, $\{|\uparrow\uparrow\rangle, |\uparrow\downarrow\rangle, |\downarrow\uparrow\rangle, |\downarrow\downarrow\rangle\}$, has the structure

$$\begin{pmatrix} u & 0 & 0 & 0 \\ 0 & w_1 & y^\star & 0 \\ 0 & y & w_2 & 0 \\ 0 & 0 & 0 & v \end{pmatrix} \tag{25}$$

The concurrence C_{ij}, a measure of the entanglement between a pair of spins at sites i and j, is given by [9, 10],

$$C_{ij} = 2\ max\left(0, |y| - \sqrt{uv}\right) \tag{26}$$

Figures 3(a) and 3(b) show the variation of C_{AC} and C_{AB} versus x. The analytical expressions for the concurrences are;

$$\begin{aligned} C_{AC} = C_{BC} &= 2\ max\left(0, \left|\tfrac{R}{A^2}\right| - \tfrac{1}{2A^2}\right) \\ C_{AB} &= 2\ max\left(0, \left|\tfrac{1}{A^2}\right| - \tfrac{R^2}{2A^2}\right) \end{aligned} \tag{27}$$

The variation of C_{BC} as a function of x is identical with that of C_{AC}. We remind ourselves that A and B are the boundary spins and C the central spin. A jump in the magnitude of the concurrence indicates a first order QPT [11, 12, 13, 14] which, as already mentioned, occurs at $x = -2$. C_{AC} and C_{BC} both become zero at $x = 1$ due to the separability of the ground state density matrix and then rises as x is increased to attain a saturation value $C_{AC} = \frac{1+2\sqrt{3}}{6+2\sqrt{3}}$ for large x. The entanglement between the boundary spins, however, has a non-zero value only for negative values of x and that too in a restricted range of x values.

We next consider the case of non-zero magnetic field ($y \neq 0$). Figure 4 shows the plots of the two lowest energies, E_5 and E_8, versus x for $y = 0.5$. One finds that a first-order QPT occurs at a specific value of $x = x_c \left(= -\sqrt{\frac{1}{2}} - \sqrt{\frac{7}{12}}\right)$ indicating a change in the nature of the ground state. Figure 5 shows the variation of E_5 and E_8 as a function of y for $x = 0.5$. Again, one notes the occurrence of a first-order QPT at a specific value of $y = y_c$. The external magnetic field removes the ground state degeneracy of the zero-field case and the three-qubit system has a unique ground state. Figures 6(a) and 6(b) show the variation of the concurrences C_{AC} and C_{AB} versus x for $y = 0.5$. In this case, the analytical expressions for the concurrences are;

$$\begin{aligned} C_{AC} = C_{BC} &= 2\ max\left(0, \left|\tfrac{R}{A^2}\right|\right) \\ C_{AB} &= 2\ max\left(0, \left|\tfrac{1}{A^2}\right|\right) \end{aligned} \tag{28}$$

In zero magnetic field ($y = 0$), the next-nearest-

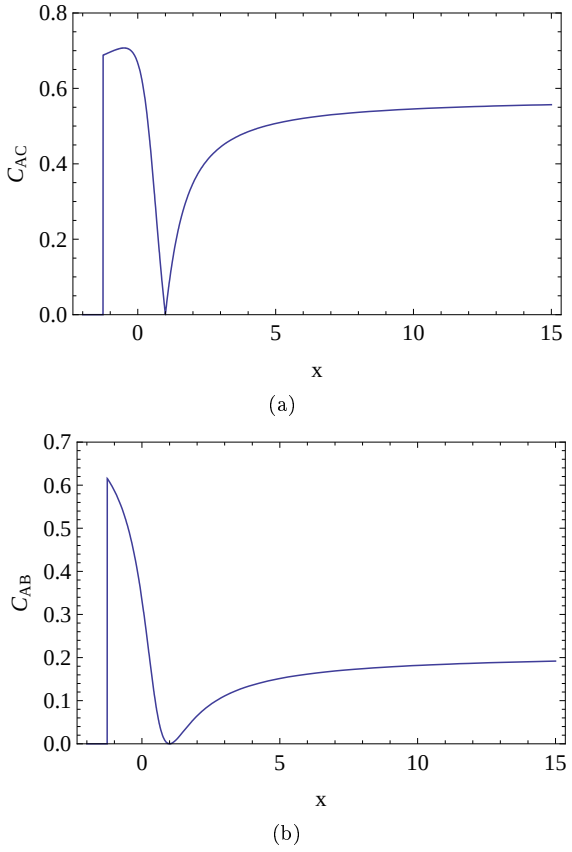

Figure 6: Variation of concurrences (a) C_{AC} and (b) C_{AB} versus x for $y = 0.5$.

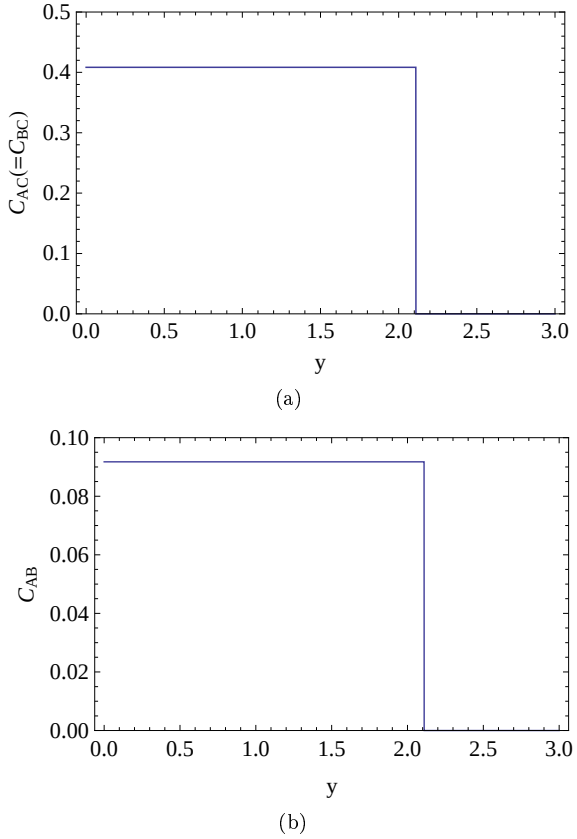

Figure 7: Variation of concurrences (a) C_{AC} and (b) C_{AB} versus y for $x = 0.5$.

neighbour (nnn) concurrence C_{AB} has non-zero values only in a restricted range of negative x values (figure 3(b)) whereas in the presence of a magnetic field ($y \neq 0$), C_{AB} is non-zero in a range of both negative and positive x values. The magnitude of the nnn entanglement is less than that of the nn entanglement for both $y = 0$ and $y \neq 0$. As y increases, one finds that x_c, the first order QPT point shifts towards more positive values. For sufficiently high values of y, entanglement exists only for positive values of x. This is so provided y is less than the critical value y_c (which depends upon x) at which a first-order QPT takes place to a separable ground state. Figures 7(a) and 7(b) show the plots of the nn and nnn concurrences, $C_{AC}(= C_{BC})$ and C_{AB} respectively versus y for $x = 0.5$. The concurrences have constant values for $y < y_c$, the QPT point, and jump discontinuously to zero values at $y = y_c$. As x increases, the value of y_c also increases. In the case of non-zero magnetic field, $y \neq 0$, the ground state is non-degenerate and the density matrix represents a pure state. In this case, the one-tangle τ_1(defined in equation (7)) can be calculated. For any choice of the central spin, the residual entanglement involving three spins is found to be zero so that only pairwise entanglement exists in the ground state. The ground states thus belong to the class of W rather than GHZ states.

III. THERMAL STATE ENTANGLEMENT

We next discuss the finite-temperature entanglement properties of the molecular three-qubit system. The thermal density matrix $\rho(T) = \frac{1}{Z}\exp(-\beta H)(\beta = \frac{1}{T}, k_B = 1)$ now replaces the ground state density-matrix with Z denoting the partition function of the system. The reduced density matrix $\rho_{ij}(T)$ has the same form as in equation (26) with $C_{ij}(T)$ given by [15]

$$C_{ij}(T) = \frac{2}{Z}\, max\left(0, |y(T)| - \sqrt{u(T)v(T)}\right) \qquad (29)$$

For the three-qubit system, the thermal density matrix is

$$\rho(T) = \frac{1}{Z}\sum_{k=1}^{8} \exp(-\beta E_k)|\psi_k\rangle\langle\psi_k| \qquad (30)$$

where the $|\psi_k\rangle$'s and E_k's are given in Eqs. (10)-(17) for the general case $y \neq 0$. When $y = 0$, the energy eigenvalues are as shown in equation (23). We first consider the

case of zero magnetic field ($y = 0$). The matrix elements u, v and y of the reduced density matrix $\rho_{AC}(T)$ are

$$u = v = \left(e^{\frac{-E_1}{T}} + \frac{1}{A^2} e^{\frac{-E_3}{T}} + \frac{1}{B^2} e^{\frac{-E_4}{T}} + \frac{1}{2} \right) \tag{31}$$

$$y = y^\star = \left(-\frac{2R}{A^2} e^{-\frac{E_3}{T}} - \frac{2S}{B^2} e^{-\frac{E_4}{T}} \right) \tag{32}$$

The reduced density matrix $\rho_{BC}(T)$ has the same matrix elements as in equations (31) and (32). For the nnn concurrence, C_{AB}, the matrix elements of the reduced density matrix are :

$$u = v = \left(e^{\frac{-E_1}{T}} + \frac{R^2}{A^2} e^{\frac{-E_3}{T}} + \frac{S^2}{B^2} e^{\frac{-E_4}{T}} \right) \tag{33}$$

$$y = y^\star = \left(\frac{2}{A^2} e^{-\frac{E_3}{T}} + \frac{2}{B^2} e^{-\frac{E_4}{T}} - 1 \right) \tag{34}$$

Figures 8(a) and 8(b) show the plots of C_{AC} and C_{AB} respectively as a function of x for different values of the temperature T. As T increases, the range of x values for which $C_{AC} \neq 0$ shifts towards more positive values. Figures 9(a) and 9(b) show C_{AC} and C_{AB} versus T for negative values of x. One can obtain similar plots for C_{AC} when x is > 0. For both the nn and nnn entanglements, one can define threshold temperatures $T_C^{(1)}$ and $T_C^{(2)}$ respectively, beyond which the concurrences [8, 16] have zero values. Figures 10(a) and 10(b) show how $T_C^{(1)}$ and $T_C^{(2)}$ vary with x for different values of y.

For non-zero magnetic field, $y \neq 0$, the matrix elements of the reduced density matrix $\rho_{AC}(= \rho_{BC})$ are given by,

$$u = \left(e^{-\frac{E_1}{T}} + \frac{1}{2} e^{-\frac{E_2}{T}} + \frac{1}{A^2} e^{-\frac{E_3}{T}} + \frac{1}{B^2} e^{-\frac{E_4}{T}} \right) \tag{35}$$

$$v = \left(e^{-\frac{E_8}{T}} + \frac{1}{2} e^{-\frac{E_7}{T}} + \frac{1}{A^2} e^{-\frac{E_5}{T}} + \frac{1}{B^2} e^{-\frac{E_6}{T}} \right) \tag{36}$$

$$y = y^\star = \left(-\frac{R}{A^2} e^{-\frac{E_3}{T}} - \frac{S}{B^2} e^{-\frac{E_4}{T}} - \frac{R}{A^2} e^{-\frac{E_5}{T}} - \frac{S}{B^2} e^{-\frac{E_6}{T}} \right) \tag{37}$$

The corresponding matrix elements for the nnn reduced density matrix are:

$$u = \left(e^{-\frac{E_1}{T}} + \frac{R^2}{A^2} e^{-\frac{E_3}{T}} + \frac{S^2}{B^2} e^{-\frac{E_4}{T}} \right) \tag{38}$$

$$v = \left(e^{-\frac{E_8}{T}} + \frac{R^2}{A^2} e^{-\frac{E_5}{T}} + \frac{S^2}{B^2} e^{-\frac{E_6}{T}} \right) \tag{39}$$

$$y = y^\star = -\frac{1}{2} \left(e^{-\frac{E_2}{T}} + e^{-\frac{E_7}{T}} \right) + \frac{1}{A^2} \left(e^{-\frac{E_3}{T}} + e^{-\frac{E_5}{T}} \right) + \frac{1}{B^2} \left(e^{-\frac{E_4}{T}} + e^{-\frac{E_6}{T}} \right) \tag{40}$$

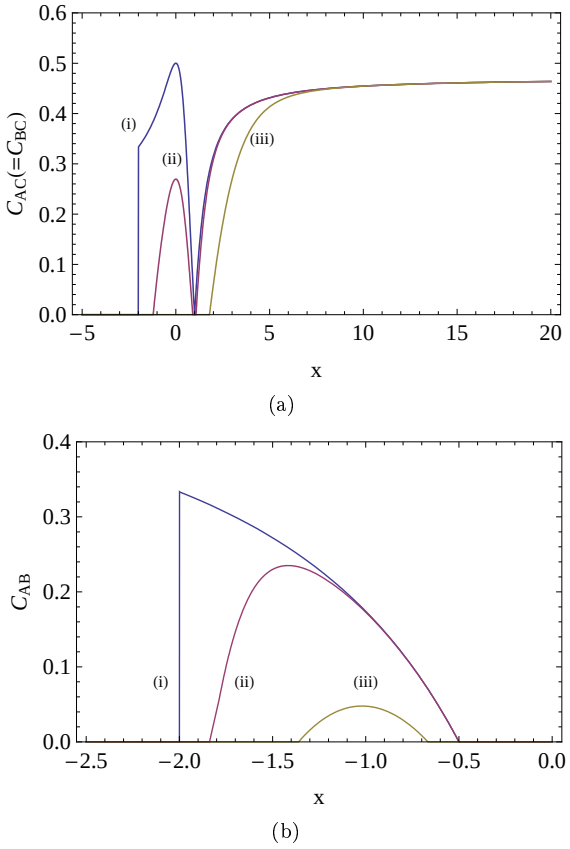

Figure 8: Variation of concurrences (a) C_{AC} and (b) C_{AB} versus x at different temperatures T with $y = 0$. The different temperature values are **(a)** (i) $T = 0$, (ii) $T = 0.5$, (iii) $T = 1.5$ and **(b)** (i) $T = 0$, (ii) $T = 0.1$, (iii) $T = 0.3$

Figures 11(a) and 11(b) show the plots of the nn and nnn entanglements, C_{AC} and C_{AB} respectively, versus x for $y = 0.5$ and at different values of T. Figure 12(a) shows the plot of C_{AC} versus T for different negative values of x with $y = 0.5$. Similar plots are obtained in other ranges of x values. Figure 12(b) shows how C_{AB} varies as a function of T.

We lastly calculate the entanglement gap temperature [17, 18], T_E, as a function of x for both zero and non-zero y. T_E is determined from the relation $U(T_E) = E_{sep}$, where $U(T) \left(= -\frac{1}{Z} \frac{\partial Z}{\partial \beta} \right)$ is the thermal energy at temperature T and E_{sep} is the ground state energy of the classical spin model corresponding to the three-qubit Hamiltonian in equation (5). E_{sep} can be easily calculated, e.g., $E_{sep} = \frac{1}{2}(-1 - 2x - y)$ for $x \geq 0$. For temperature $T < T_E$, the thermal state is entangled. Figure 13 exhibits the variations of T_E versus x for different values of y.

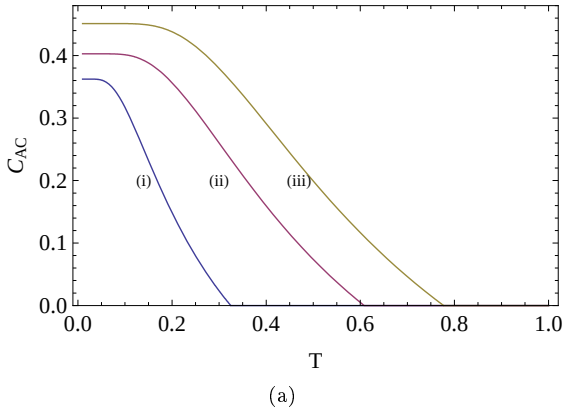

(a)

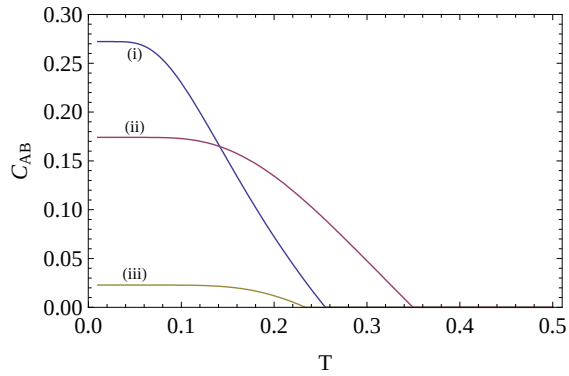

(b)

Figure 9: Variation of concurrences (a) C_{AC} and (b) C_{AB} versus T for different negative values of x with $y = 0$. The different x values are (i) $x = -1.5$, (ii) $x = -1$, and (iii) $x = -0.55$ for both (a) and (b).

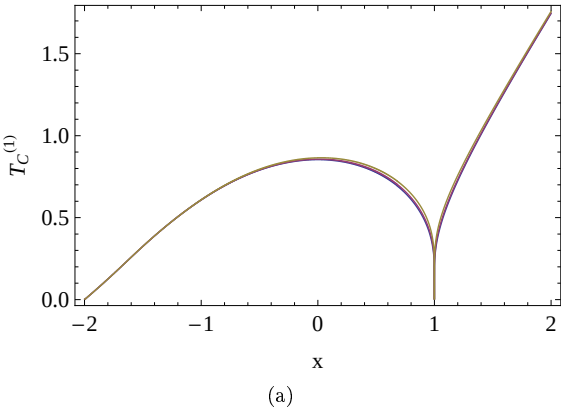

(a)

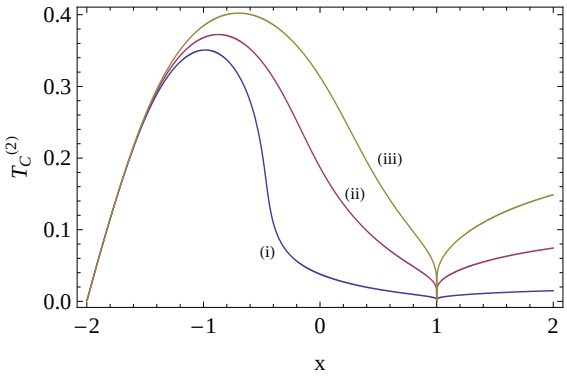

(b)

Figure 10: The threshold entanglement temperature (a) $T_C^{(1)}$ versus x for nn entanglement and (b) $T_C^{(2)}$ versus x for nnn entanglement with (i) $y = 0.1$ (ii) $y = 0.5$ and (iii) $y = 1$. $T_C^{(1)}$ has a very weak dependence on the values of y.

IV. SUMMARY AND DISCUSSION

In this paper, we have obtained quantitative measures of pairwise entanglement in a molecular three-qubit system as a function of two parameters x and y. The system represents the recently engineered Cr_7Ni-Cu^{2+}-Cr_7Ni complex consisting of two Cr_7Ni rings coupled via a central Cu^{2+} ion. The parameters x and y appearing in the qubit Hamiltonian (equation (9)) have their origins in an effective Cu-ring axial exchange due to the projection of the rings' dipolar and crystal-field anisotropies and an external magnetic field respectively. Timco *et al* [3] have provided an experimental demonstration that the coupling between molecular spin clusters can be manipulated by altering the nature of the linker ions. This opens up the possibility of chemically controlling the generation of entanglement in spin systems. The molecular three-qubit system studied in this paper belongs to a family of clusters with AFM exchange interactions between the nn ions and a spin-$\frac{1}{2}$ ground state. The simplest case is that of a finite chain with an odd number of $S = \frac{1}{2}$ spins and dominant AFM interactions between the nn spins. An alternative way of obtaining an $S = \frac{1}{2}$ ground state is to replace a single spin in an AFM chain, containing an even number of spins, by a spin of different magnitude such that the ground state spin is of magnitude $\frac{1}{2}$. The Cr_7Ni ring provides an example of the latter possibility.

In general, the arrangement of spins in a chain can be either linear, or cyclic. The molecular three-qubit system studied in this paper is a linear-chain complex, whereas the three qubit chain studied in [8] is cyclic in nature. Cyclic spin chains with an odd number of antiferromagnetically coupled spins have degenerate ground states due to magnetic frustration. For a three-spin cyclic chain, the anisotropic Heisenberg XXZ model has a four-fold degenerate ground state in zero magnetic field [8]. In the presence of an external magnetic field, the ground state is doubly degenerate. The effective three-qubit Hamiltonian (equation (9)) has the form of the anisotropic Heisenberg XXZ Hamiltonian but with a linear i.e. an open-ended structure. In this case, the ground state is doubly degenerate in zero magnetic field ($y = 0$) and non-degenerate when $y \neq 0$. The cyclic chain has a greater ground state degeneracy because of frustration.

There are prominent differences in the entanglement

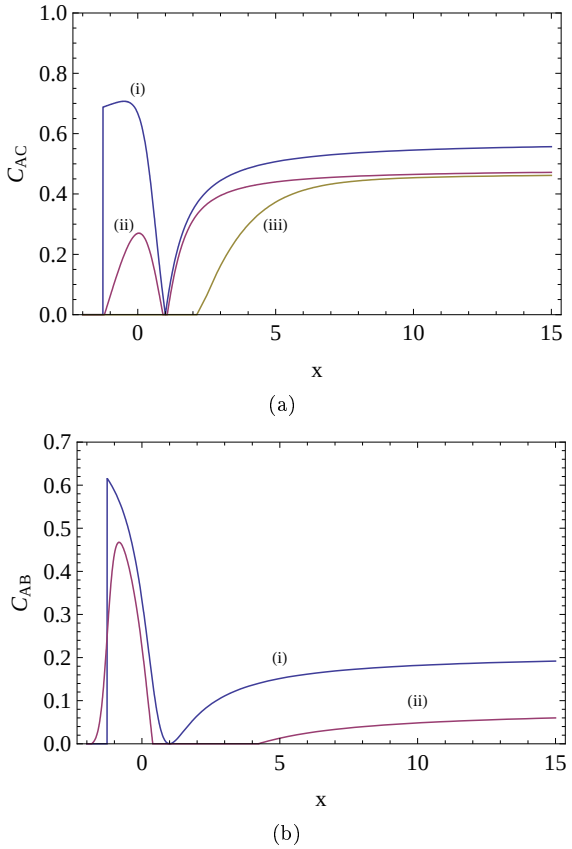

Figure 11: Variation of concurrences (a) C_{AC} and (b) C_{AB} versus x at different temperatures T with $y = 0.5$. The different temperature values are **(a)** (i) $T = 0$, (ii) $T = 0.5$, (iii) $T = 2$ and **(b)** (i) $T = 0$, (ii) $T = 0.5$

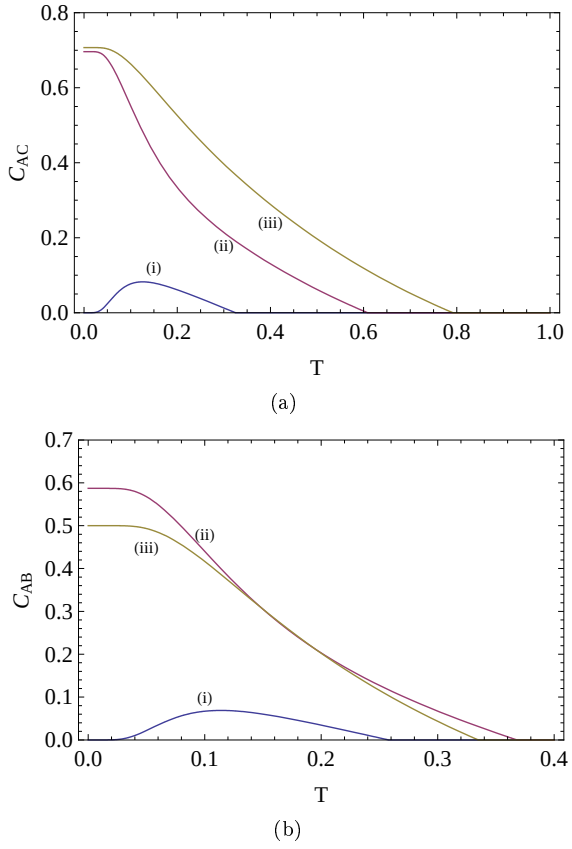

Figure 12: Variation of concurrences (a) C_{AC} and (b) C_{AB} versus T for different negative values of x with $y = 0.5$. The different values of x are (i) $x = -1.5$, (ii) $x = -1$, and (iii) $x = -0.5$ for both (a) and (b).

features of cyclic and linear spin chains. As shown in [8], in the case of the AFM cyclic XXZ model, there is no pairwise entanglement, as measured by concurrence, for all values of the anisotropy constant. At $T = 0$ also, the concurrence is zero for the AFM case. In contrast, the AFM linear chain has pairwise entanglement at both $T = 0$ and $T \neq 0$ (figures 3 and 8). One now distinguishes between nn and nnn entanglements. In the AFM case, the nnn concurrence C_{AB} is zero at zero and finite temperatures whereas the nn concurrence $C_{AC}(= C_{BC})$ is non-zero at both $T = 0$ and $T \neq 0$. Comparing figures 3 and 6, one finds that on inclusion of the magnetic field the range of x values for which C_{AB} (the nnn concurrence) is $\neq 0$ is considerably extended. For a specific value of x, there is, however, a critical value of y_c of y such that the pairwise entanglement vanishes when $y > y_c$. Earlier studies [8, 10] have shown that the entanglement between two spins in an AFM chain can be increased by raising the temperature or the external magnetic field in specific ranges. This is true for our three-qubit system also. In figures 12(a) and 12(b), the curve (i) shows the increase of both C_{AC} and C_{AB} with temperature T. We have further shown that only pairwise entanglement exists in the ground state with $y \neq 0$, i.e., there is no three-qubit entanglement as exists in the GHZ state (equation (6)). One interesting feature of the linear three-spin chain relates to the variation of the threshold entanglement temperatures $T_C^{(1)}$ and $T_C^{(2)}$ versus x for different values of y. As shown in figure 10(a), the $T_C^{(1)}$ versus x plot depends weakly on the values of y. The threshold temperature $T_C^{(2)}$, for nnn entanglement, however, varies more prominently with y. In the case of the cyclic chain, the single threshold temperature depends on both x and y. As shown in figure 13, the plots of the entanglement gap temperature, T_E, versus x are different for different values of y. In fact, T_E has a non-monotonic dependence on the values of y (the $y = 1$ curve lies in between the $y = 0.1$ and $y = 0.5$ curves). One further notes, from figures 10 and 13, that the entanglement gap and threshold temperatures are different for the same values of the parameters x and y. In fact, one finds that $T_C^{(2)} < T_E < T_C^{(1)}$. Figures 4-7 and Figures 11-12 have been obtained by fixing either x or y at a specific value. The observations are, however, general in nature and hold true in extended ranges of x and y values. In the model studied by us, we

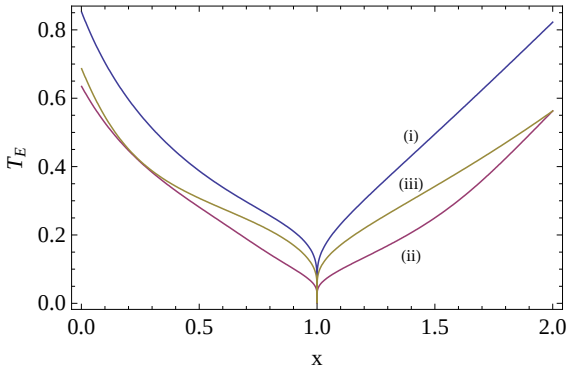

Figure 13: Variation of the entanglement gap temperature, T_E , versus x for different magnetic fields. The different values of y are (i) $y = 0$, (ii) $y = 0.5$, and (iii) $y = 1$

have assumed that the gyromagnetic factors g_A, g_B, g_C are of equal amplitude g (equation (8)). In the case of the engineered three-qubit system, the diagonal tensors $g_{A,B}$ and g_C are different. Assuming $g_A = g_B \neq g_C$, ($g_{C(zz)} = 2.07$, $g_{A,B(zz)} = 1.79$, as quoted in [3]), we find no qualitative changes in the results reported in sections 2 and 3. It will be of interest to study the general case of the magnetic field pointing in an arbitrary direction.

The three-qubit molecular cluster exhibits first-order QPTs at specific values of x and y. In figure 3(a), the QPT at $x = -2$ separates two phases, for $x < -2$ the ground state has no entanglement whereas for $-2 < x < 1$, the ground state, described by the mixed state in equation (24), has pairwise entanglement. Similarly, as shown in figure 7, a first order QPT occurs at $y = y_c$. The point $x = 1$ is of special interest as the ground and thermal states become separable at this point. The threshold entanglement temperatures, $T_C^{(1)}$ and $T_C^{(2)}$, drop sharply to zero at $x = 1$. The first-order transition points can be shifted by changing the parameters x and y. For example, the transition point x_c can be shifted towards higher values by increasing y. The first order QPTs are marked by discontinuities in the magnitude of both the nn and nnn concurrences associated with the ground states. The molecular three-qubit system, Cr_7Ni-Cu^{2+}-Cr_7Ni, has been specifically engineered with QIP applications in mind. Since entanglement is a fundamental resource in such applications, a knowledge of its dependence on the relevant parameters of the system will be of use in the designing and implementation of QIP protocols. With possibilities for controlling the couplings in molecular qubit systems [3] and realizations of spin Hamiltonians in optical lattices [19], some of the theoretical results could be observed in actual experiments.

Acknowledgement : The Authors thank Amit Tribedi for some useful discussions.

[1] M. A. Nielsen and I. L. Chuang. Quantum Computation and Quantum Information (Cambridge University Press, Cambridge, England, 2000)
[2] M. Affronte et. al., Dalton Trans. 2810 (2006)
[3] G. A. Timco et. al., Nature Nanotechnology 4, 173 (2009)
[4] W. Dür, G. Vidal and J. I. Cirac, Phys. Rev. A 62, 062314 (2000)
[5] B. Röthlisberger, J. Lehmann, D. S. Saraga, P. Traber and D. Loss, Phys. Rev. Lett. 100, 100502 (2008)
[6] A. K. Rajagopal and R. W. Rendell, Phys. Rev. A 65, 032328 (2002)
[7] V. Coffman, J. Kundu, and W. K. Wootters, Phys. Rev. A 61, 052306 (2000)
[8] X. Wang, H. Fu, and A. I. Solomon, J. Phys. A 34, 11307 (2001)
[9] K. M. O'Connor and W. K. Wootters, Phys. Rev. A 63, 052302 (2001); W. K. Wootters, Phys. Rev. Lett. 80, 2245 (1998)
[10] M. C. Arnesen, S. Bose, and V. Vedral, Phys. Rev. Lett. 87, 017901 (2001); D. Gunlycke, V. M. Kendon, V. Vedral and S. Bose, Phys. Rev. A 64, 042302 (2001)
[11] L. -A. Wu, M. S. Sarandy and D. A. Lidar, Phys. Rev. Lett. 93, 250404 (2004)
[12] I Bose and E. Chattopadhyay, Phys. Rev. A 66, 062320 (2002)
[13] F. C. Alcaraz, A. Saguia and M. S. Sarandy, Phys. Rev. A 70, 032333 (2004)
[14] J. Vidal, R. Mosseri and J. Dukelsky, Phys. Rev. A 69, 054101 (2004)
[15] I. Bose and A. Tribedi, Phys. Rev. A 72, 022314 (2005)
[16] X. Wang, Phys. Rev. A 66, 044305 (2002)
[17] G. Tóth, Phys. Rev. A 71, 010301 (R) (2005)
[18] M. R. Dowling, A. C. Doherty and S. D. Bartlett, Phys. Rev. A 70, 062113 (2004)
[19] M. Lewenstein, A. Sanpera, V. Ahufinger, B. Damski, A. Sen(de), and U. Sen, Adv. Phys. 56, 243 (2007).